Electronic Supporting Information (ESI)

Synthesis and Molecular Structural Studies of Racemic Chiral-at-Vanadium(V) Complexes Using an Unsymmetric Achiral Phenolic Bidentate Ligand

Koichi Nagata,[1,2] Ayako Hino,[1] Hitoshi Ube,[1] Hiroyasu Sato[3] and Mitsuhiko Shionoya[1]*

[1] Department of Chemistry, Graduate School of Science, The University of Tokyo, 7-3-1 Hongo, Bunkyo-ku, Tokyo 113-0033, Japan

[2] Current address: Department of Chemistry, Graduate School of Science, Tohoku University, Aoba-ku, Sendai, Miyagi 980-8578, Japan.

[3] Rigaku Corporation, 3-9-12 Matsubara-cho, Akishima, Tokyo 196-8666, Japan.

To whom correspondence should be addressed.

shionoya@chem.s.u-tokyo.ac.jp

Synthesis of 2-adamantyl-4-*tert*-butyl-6-(3,5-di-*tert*-butyl-2-hydroxybenzyl)phenol (H_2L)

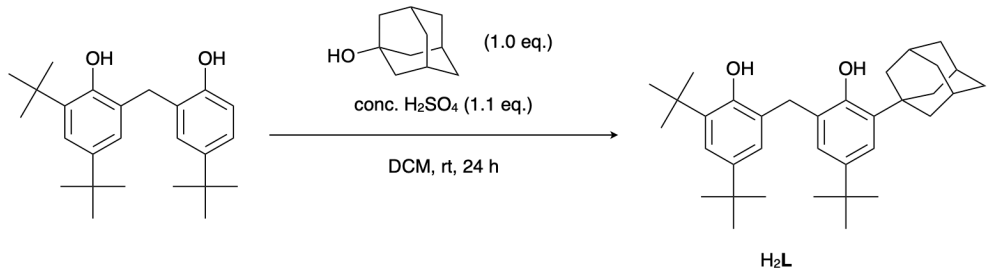

All the procedures were performed under an inert gas atmosphere. 2,4-Di-*tert*-butyl-6-(5-*tert*-butyl-2-hydroxybenzyl)phenol (97.8 mg, 266 μmol, 1.0 eq.) and 1-adamantanol (40.6 mg, 267 mmol, 1.0 eq.) were dissolved in dry dichloromethane (10 mL). Conc. sulfuric acid (15.0 μL, 281 μmol, 1.1 eq.) was added and the solution was stirred at room temperature for 24 h. The resultant red-brown solution was washed with water (10 mL) and dichloromethane (5 mL) was added. The aqueous layer was extracted with dichloromethane (5 mL × 3) and the combined organic layer was dried over sodium sulfate. After removing the solvent, H_2**L** was obtained as brown paste (103 mg, 205 μmol, 77% yield). The paste was crystallized from *n*-hexane at –20 °C to afford microcrystalline powder (32.1 mg, 63.6 μmol, 24% yield). ^{1}H NMR (500 MHz; $CDCl_3$): δ 7.19 (d, J = 2.4 Hz, 1H), 7.14 (m, 3H), 5.92 (s, 1H), 5.85 (s, 1H), 3.92 (s, 2H), 2.10 (m, 9H), 1.78 (s, 6H), 1.41 (s, 9H), 1.28 (s, 18H).; ^{13}C NMR (126 MHz; $CDCl_3$): δ 150.22, 150.11, 143.3, 143.0, 135.8, 135.6, 126.29, 126.21, 125.32, 125.12, 122.7, 41.2, 37.16, 37.06, 34.8, 34.48, 34.42, 32.7, 31.7, 30.2, 29.2; ESI-TOF-MS (low resolution, positive-mode, solvent: $CHCl_3$/MeOH): *m/z* calcd. for ([H_2**L**·Na]$^+$) [$C_{35}H_{50}O_2Na^{23}$]$^+$: 525.37; found: 525.37.

NMR spectra of H_2L

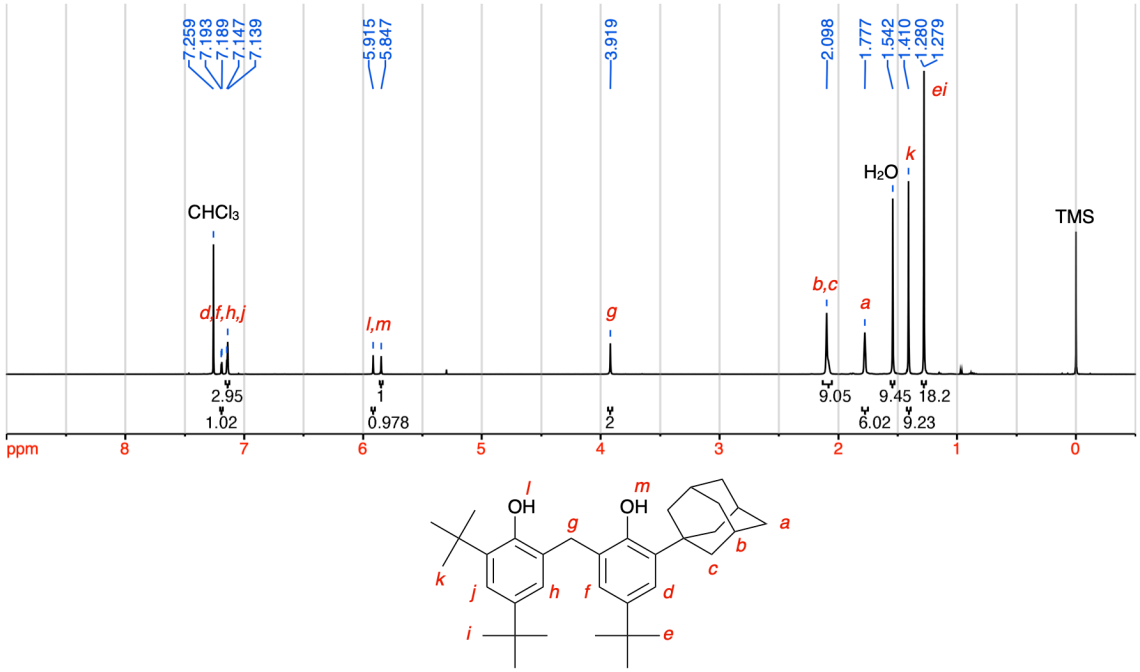

Fig. S1 ^{1}H NMR spectrum of H_2**L** (500 MHz, $CDCl_3$, 300 K).

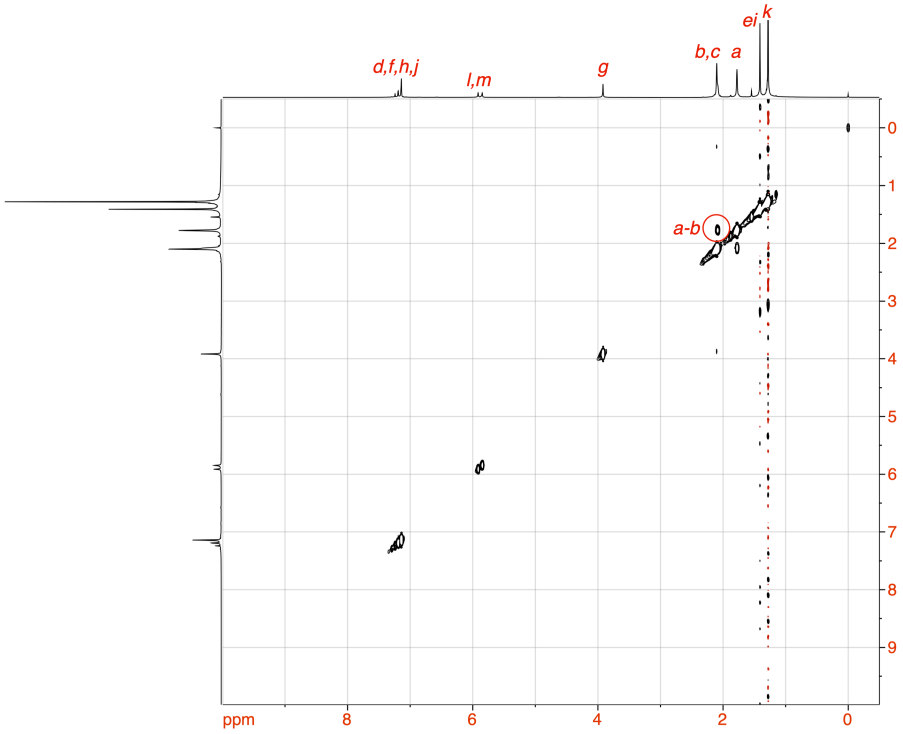

Fig. S2 ^{1}H-^{1}H COSY NMR spectrum of H_2**L** (500 MHz, $CDCl_3$, 300 K).

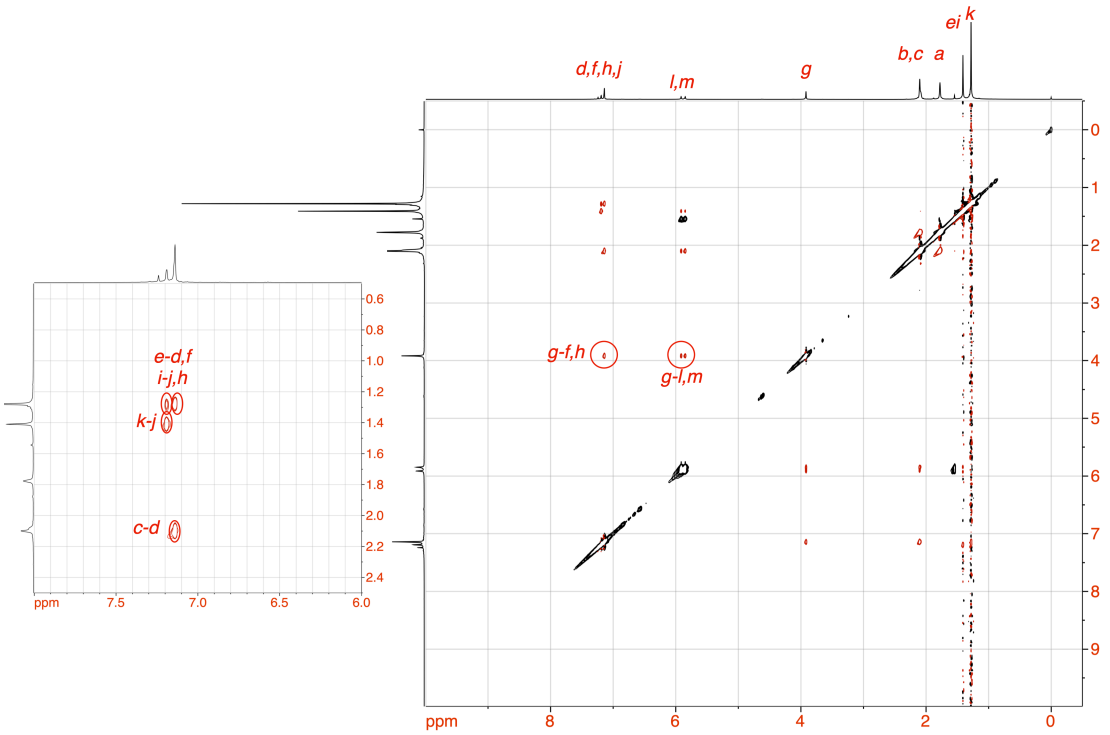

Fig. S3 ^{1}H-^{1}H NOESY NMR spectrum of H_2**L** (500 MHz, $CDCl_3$, 300 K).

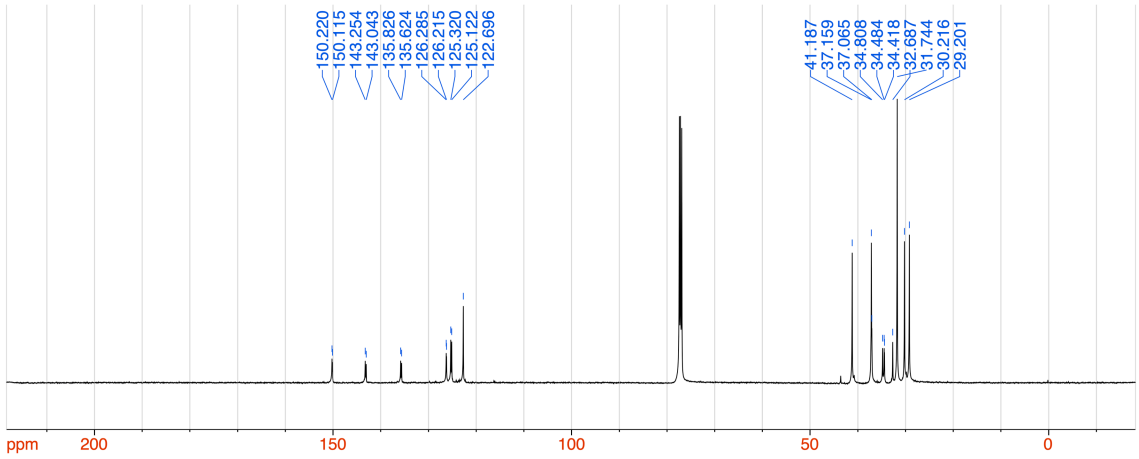

Fig. S4 ^{13}C{^{1}H} NMR spectrum of H_2**L** (126 MHz, $CDCl_3$, 300 K).

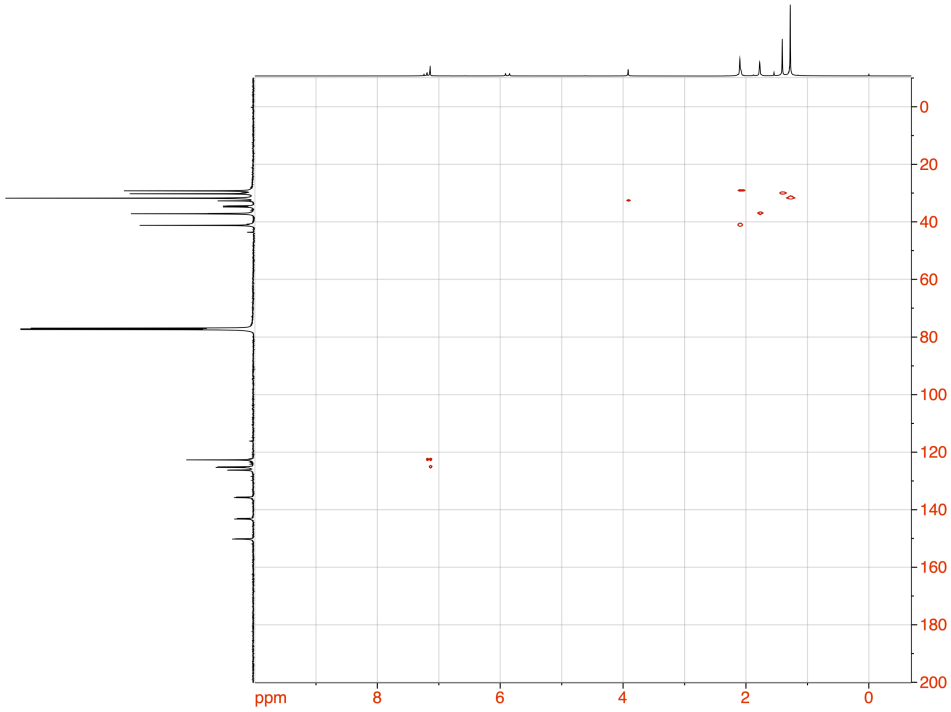

Fig. S5 HSQC NMR spectrum of H_2**L** (^{1}H: 500 MHz, ^{13}C: 126 MHz, $CDCl_3$, 300 K).

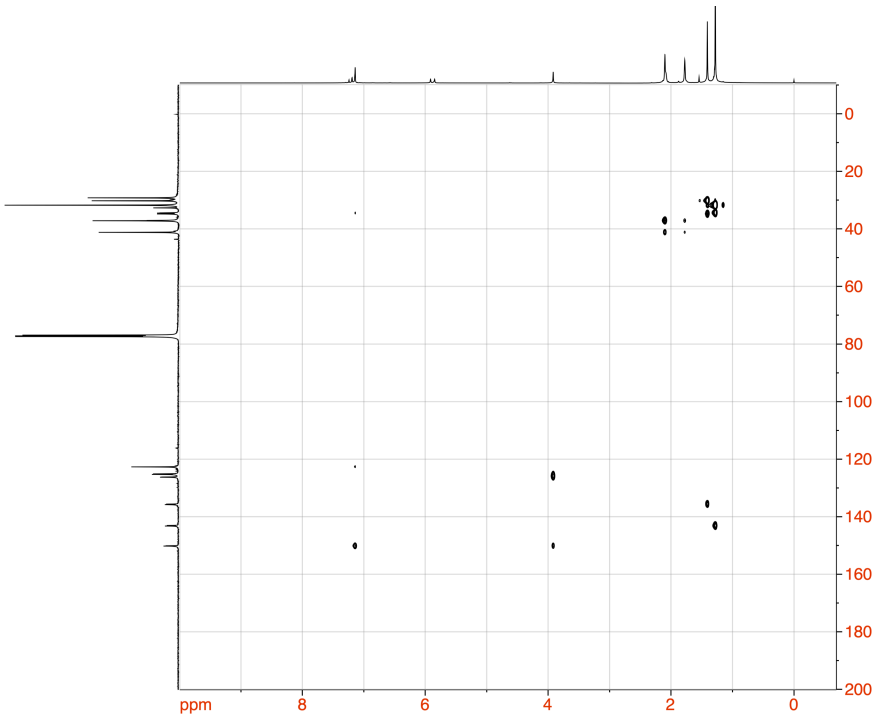

Fig. S6 HMBC NMR spectrum of H_2**L** (^{1}H: 500 MHz, ^{13}C: 126 MHz, $CDCl_3$, 300 K).

NMR spectra of [V(O)(O*t*-Bu)L] (1): complexation of H_2L with V(O)(O*t*-Bu)$_3$

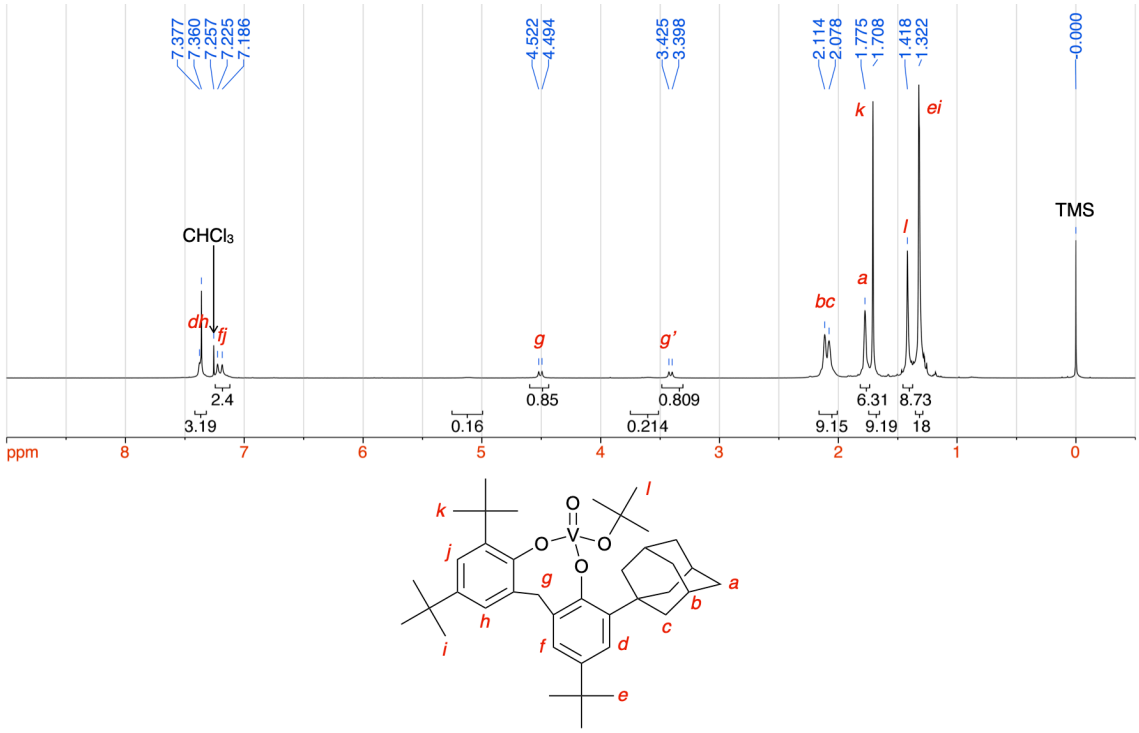

Fig. S7 ^{1}H NMR spectrum of **1** (500 MHz, $CDCl_3$, 300 K). According to DFT calculations, the major and minor signals may correspond to conformers I and II of the eight-membered ring, respectively.

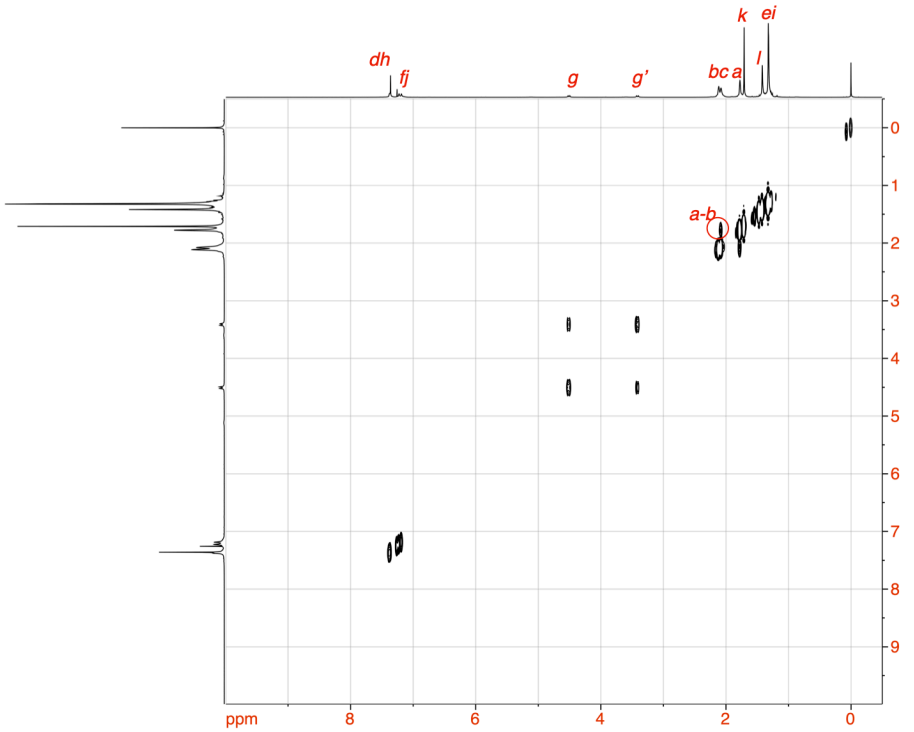

Fig. S8 ^{1}H–^{1}H COSY NMR spectrum of **1** (500 MHz, $CDCl_3$, 300 K).

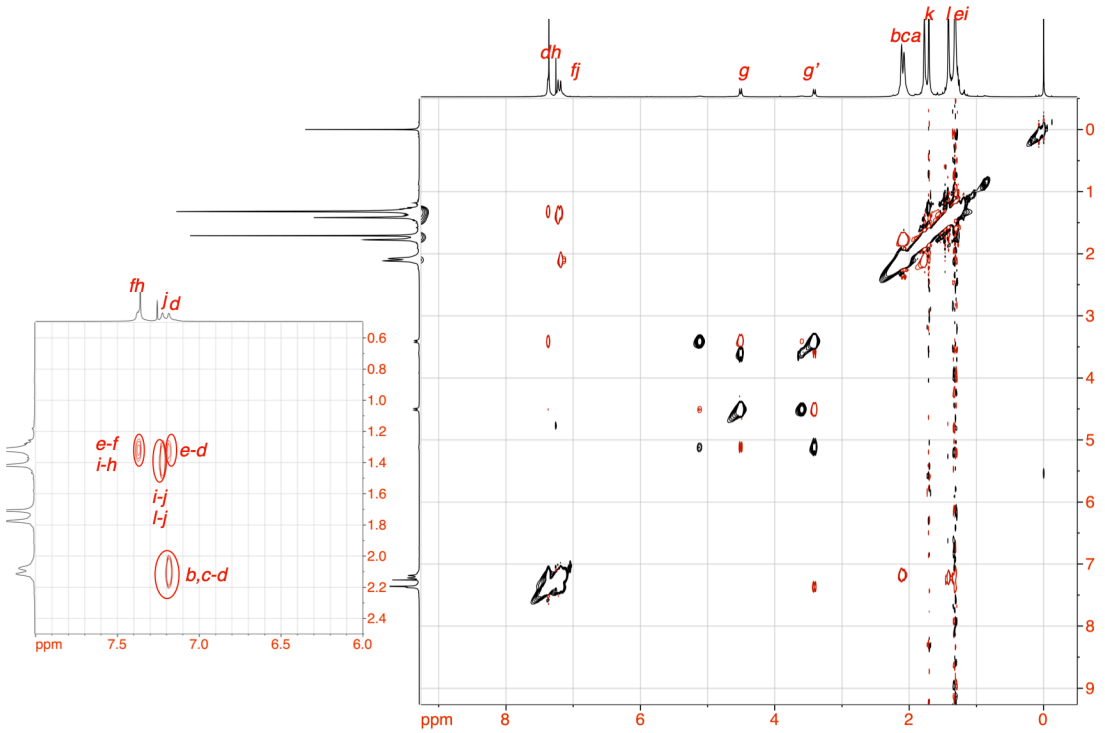

Fig. S9 ^{1}H–^{1}H NOESY NMR spectrum of **1** (500 MHz, $CDCl_3$, 300 K).

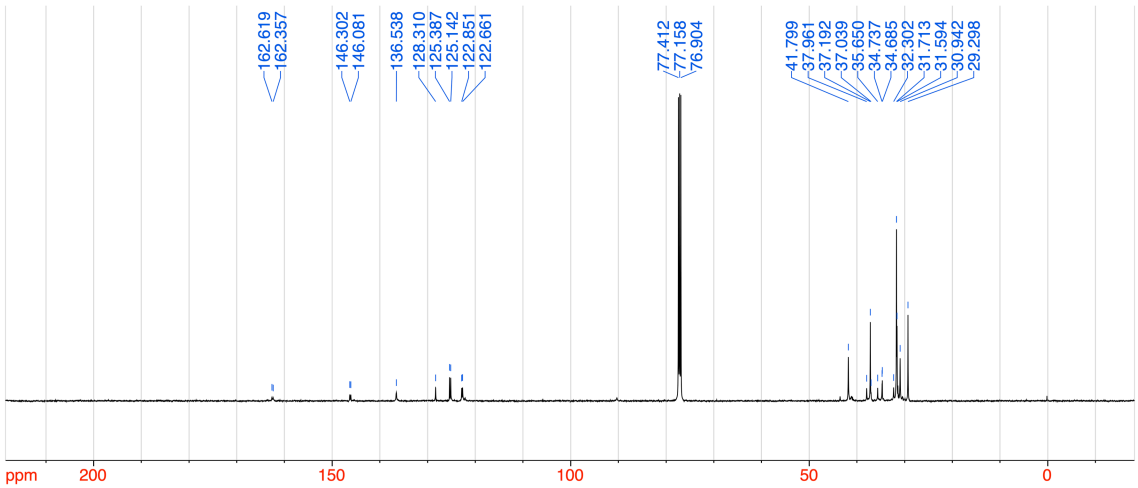

Fig. S10 ^{13}C{^{1}H} NMR spectrum of **1** (126 MHz, $CDCl_3$, 300 K).

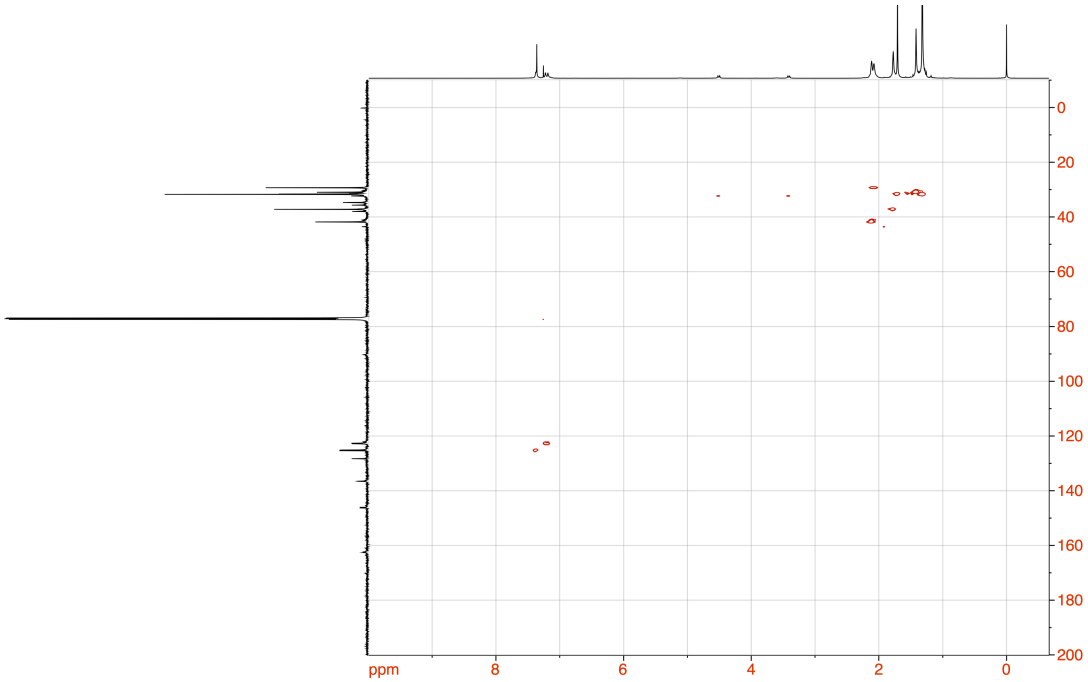

Fig. S11 HSQC NMR spectrum of **1** (^{1}H: 500 MHz, ^{13}C: 126 MHz, $CDCl_3$, 300 K).

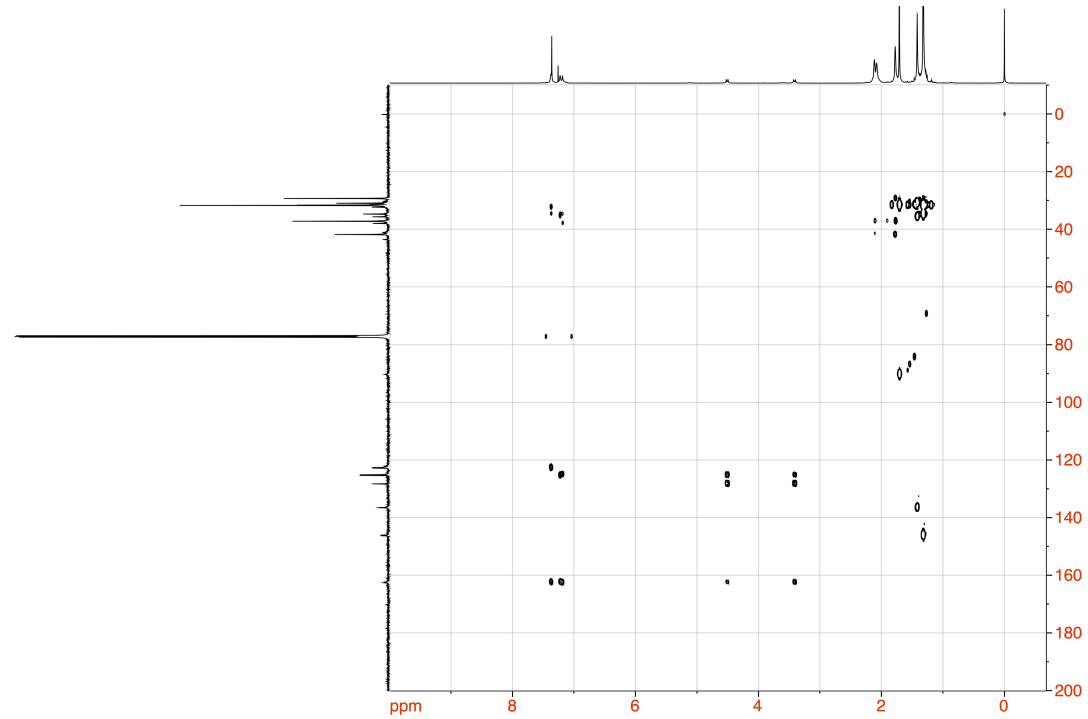

Fig. S12 HMBC NMR spectrum of **1** (^{1}H: 500 MHz, ^{13}C: 126 MHz, $CDCl_3$, 300 K).

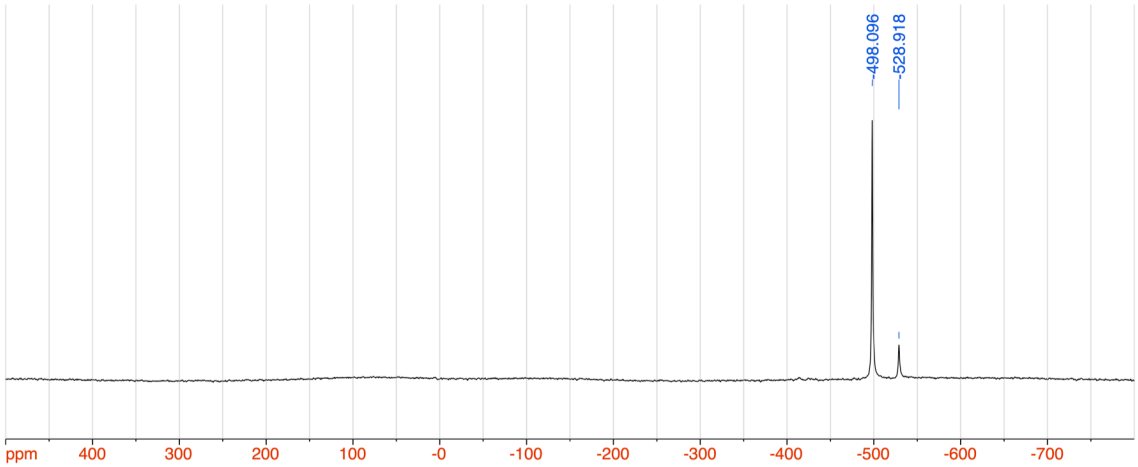

Fig. S13 ^{51}V NMR spectrum of **1** (132 MHz, $CDCl_3$, 300 K). According to DFT calculations, the major and minor signals may correspond to conformers I and II of the eight-membered ring, respectively.

NMR Spectra of [V(O)ClL] (2): complexation of H_2L with $V(O)Cl_3$

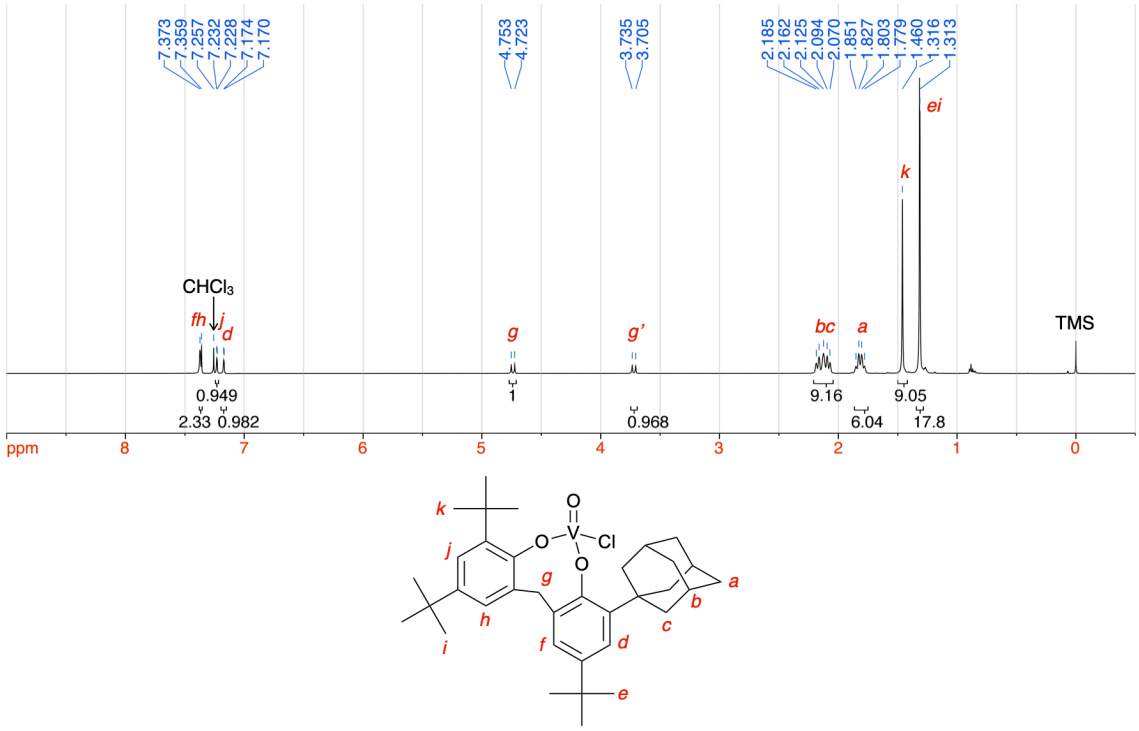

Fig. S14 ^{1}H NMR spectrum of **2** (500 MHz, $CDCl_3$, 300 K).

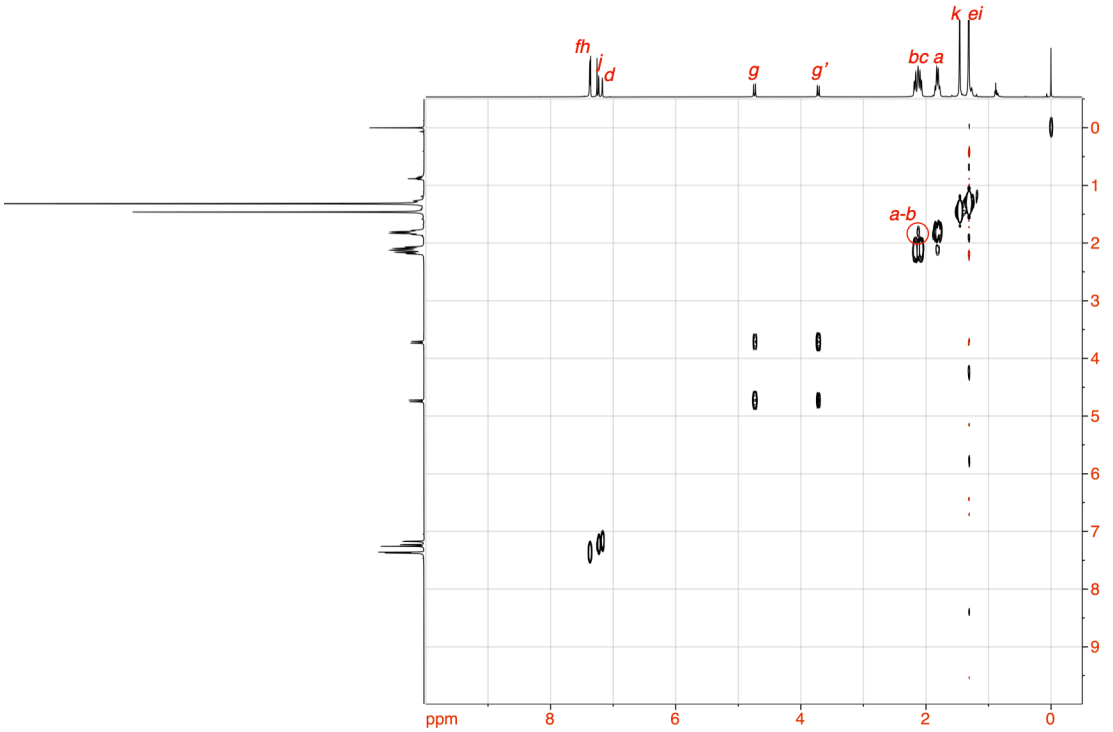

Fig. S15 ^{1}H–^{1}H COSY NMR spectrum of **2** (500 MHz, $CDCl_3$, 300 K).

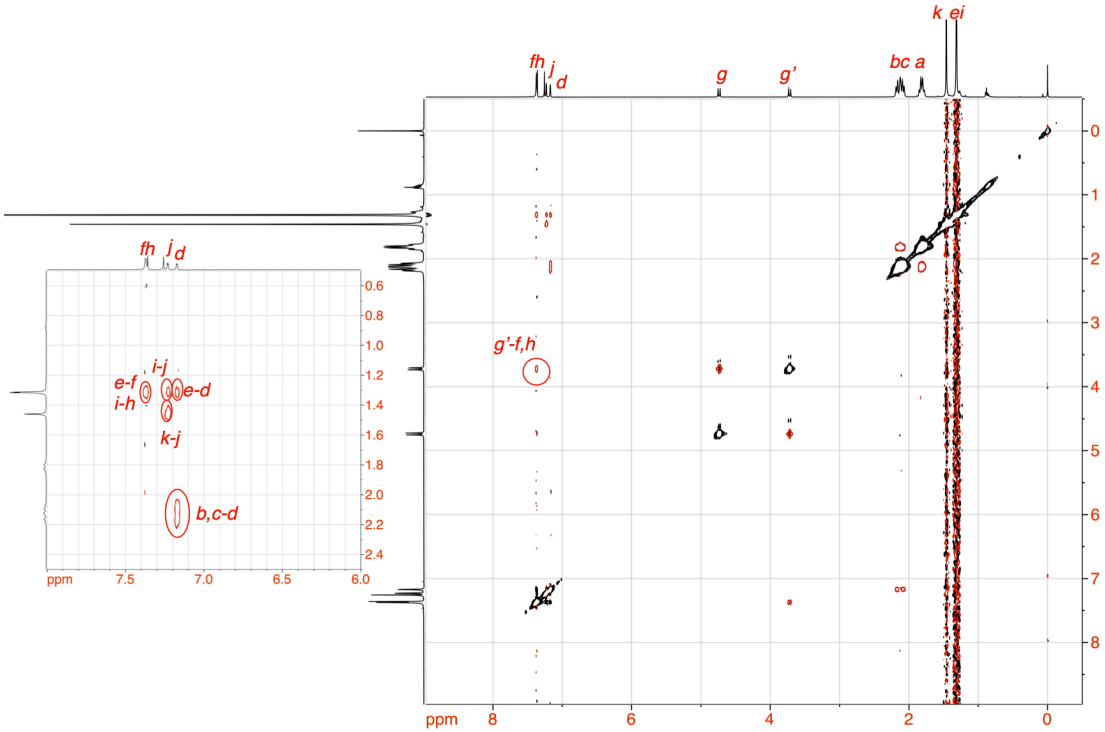

Fig. S16 $^{1}H–^{1}H$ NOESY NMR spectrum of **2** (500 MHz, $CDCl_3$, 300 K).

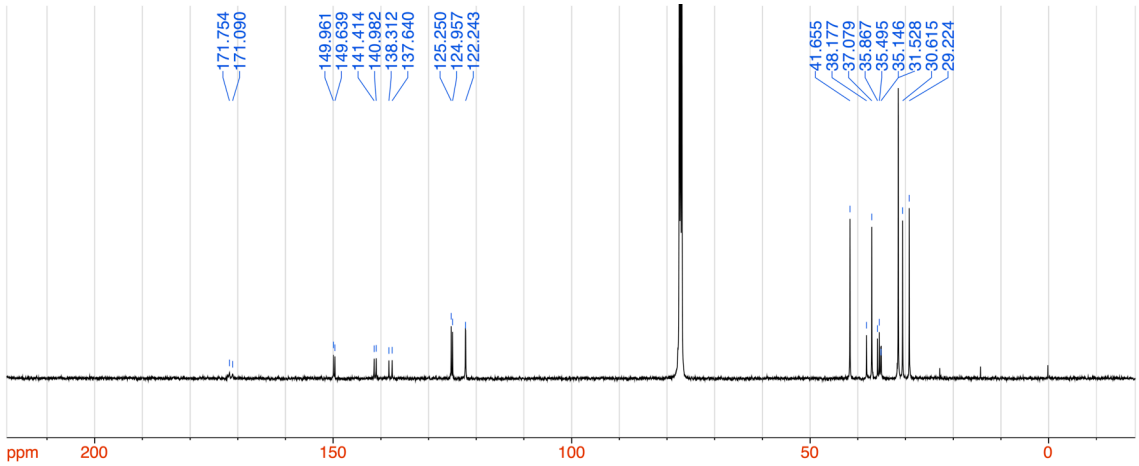

Fig. S17 $^{13}C\{^{1}H\}$ NMR spectrum of **2** ($CDCl_3$, 300 K, 126 MHz).

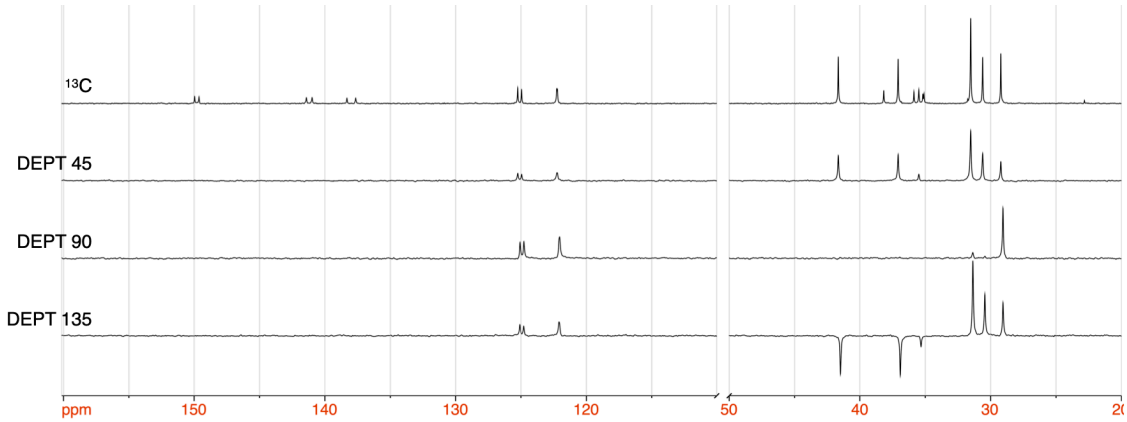

Fig. S18 DEPT 135, 90, 45, and $^{13}C\{^{1}H\}$ NMR spectrum of **2** (126 MHz, $CDCl_3$, 300 K).

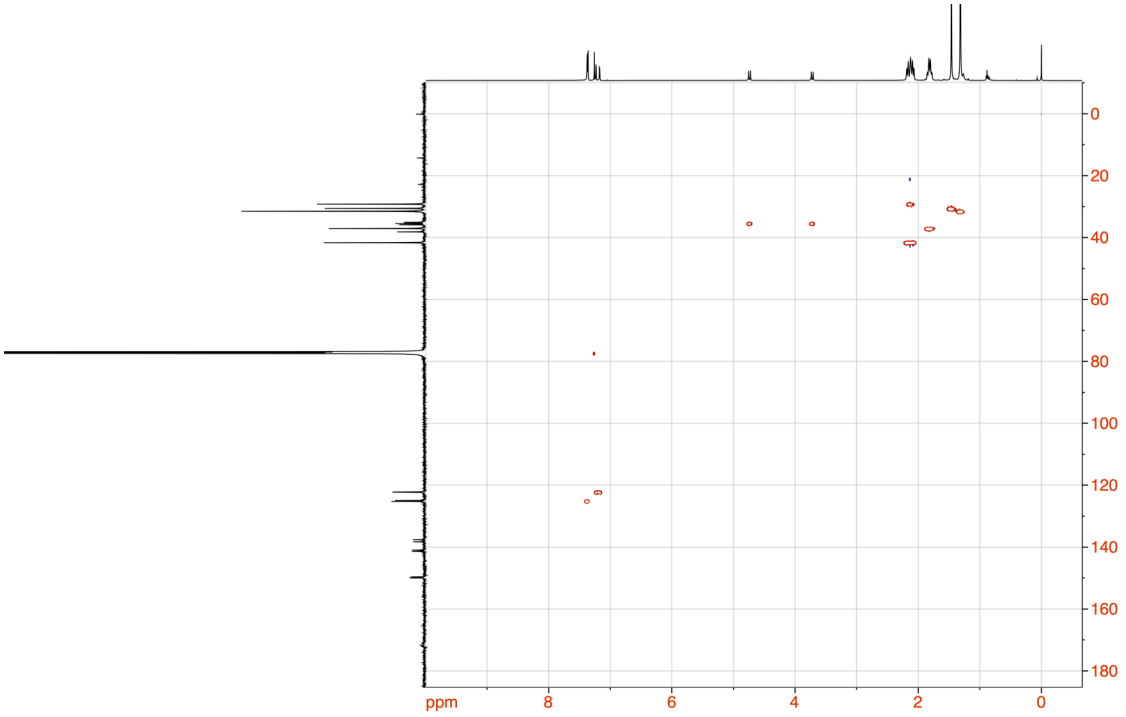

Fig. S19 HSQC NMR spectrum of **2** (^{1}H: 500 MHz, ^{13}C: 126 MHz, $CDCl_3$, 300 K).

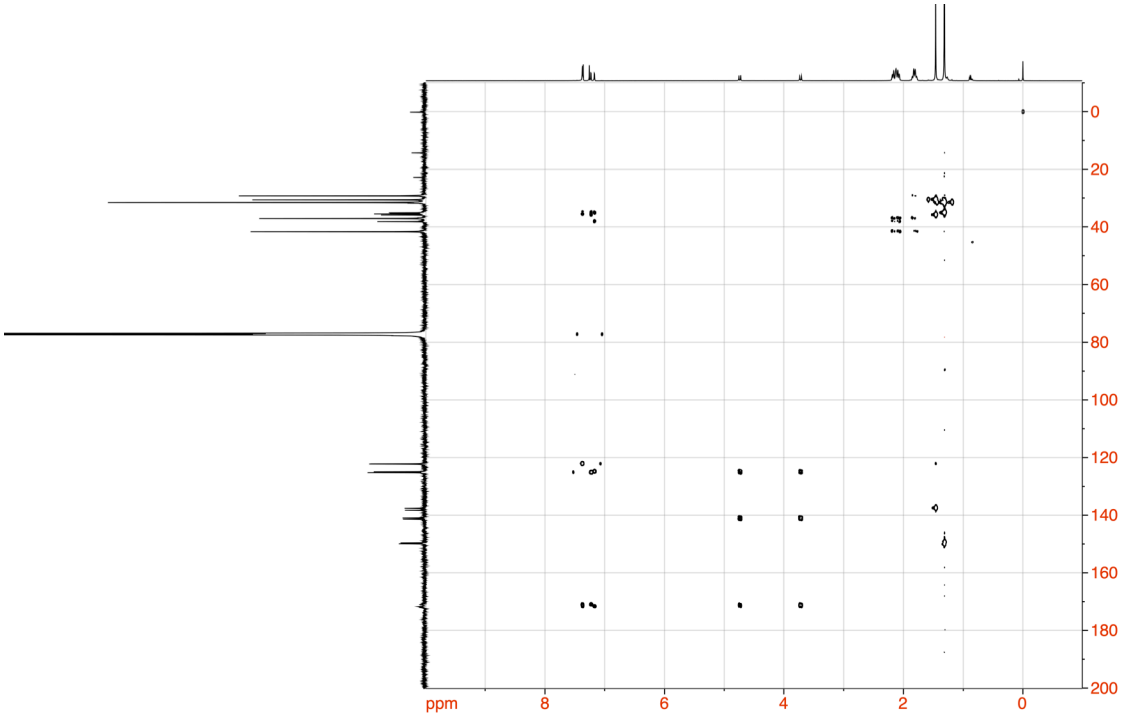

Fig. S20 HMBC NMR spectrum of **2** (^{1}H: 500 MHz, ^{13}C: 126 MHz, $CDCl_3$, 300 K).

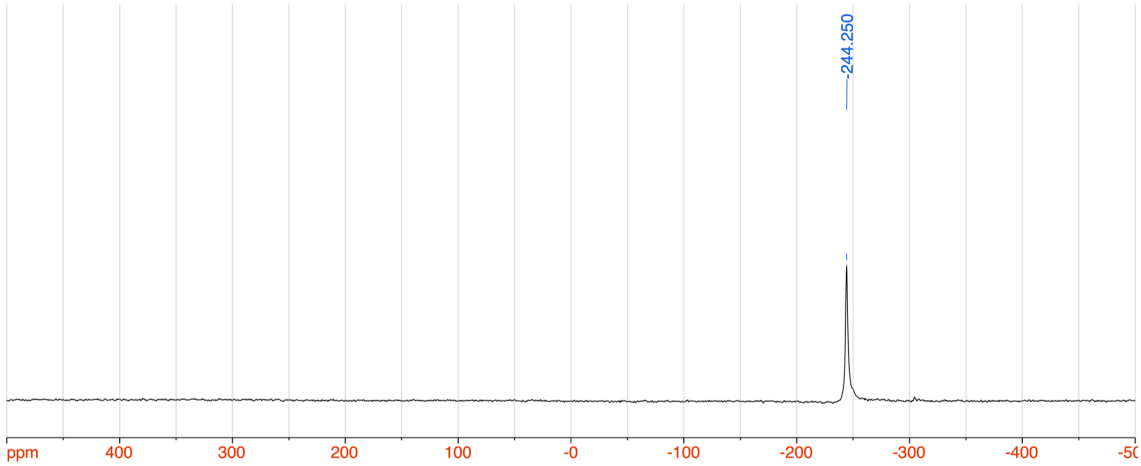

Fig. S21 ^{51}V NMR spectrum of **2** (132 MHz, $CDCl_3$, 300 K).

Synthesis of [V(O)(O*t*-Bu)L'] (3): complexation of H_2L' with V(O)(O*t*-Bu)$_3$ (H_2L' = 6,6'-methylenebis(2,4-di-*tert*-butylphenol))

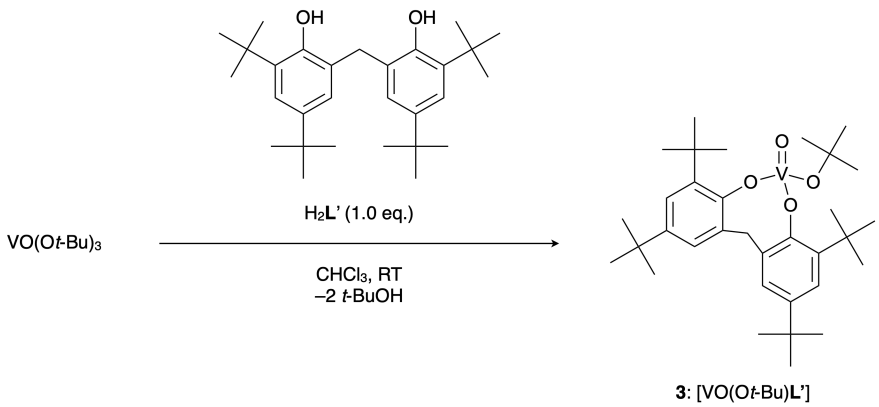

3: [VO(O*t*-Bu)**L'**]

V(O)(O*t*-Bu)$_3$ (2.2 mg, 7.3 μmol, 1.0 eq.) and H_2**L'** (3.1 mg, 7.3 μmol, 1.0 eq.) were mixed in 1 mL of $CHCl_3$ and the resultant solution was stirred at room temperature for 10 min. The solvent and *t*-BuOH generated were then removed by evaporation, 1 mL of $CHCl_3$ was added again and the solution was stirred at room temperature for 24 h. The solution was filtered through a glass fibre filter paper and the solvent was removed by evaporation to afford **3** as a brown solid (3.7 mg, 6.8 μmol, 93% yield). ^{1}H NMR (500 MHz, $CDCl_3$): δ 7.38 (s, 2H), 7.24 (s, 2H), 4.52 (d, J = 13.7 Hz, 1H), 3.41 (d, J = 13.7 Hz, 1H), 1.70 (s, 9H), 1.42 (s, 18H), 1.32 (s, 18H); ^{13}C NMR (126 MHz, $CDCl_3$): δ 162.2, 146.2, 136.5, 128.0, 125.4, 122.8, 77.4, 77.2, 76.9, 35.7, 34.7, 32.3, 31.71, 31.57, 31.0; ^{51}V NMR (132 MHz, $CDCl_3$): δ –500.2 (broad, $w_{1/2}$ ≈158 Hz).

NMR spectra of [V(O)(O*t*-Bu)L'] (3)

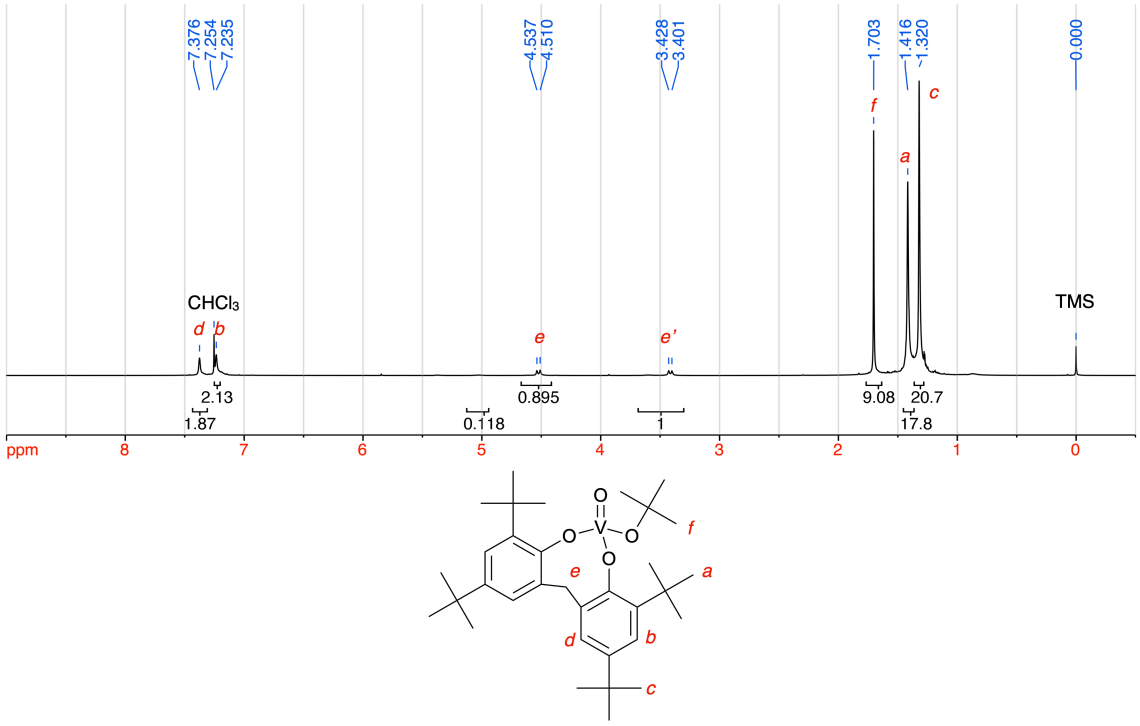

Fig. S22 ^{1}H NMR spectrum of **3** (500 MHz, $CDCl_3$, 300 K). According to DFT calculations, the major and minor signals may correspond to conformers I and II of the eight-membered ring, respectively.

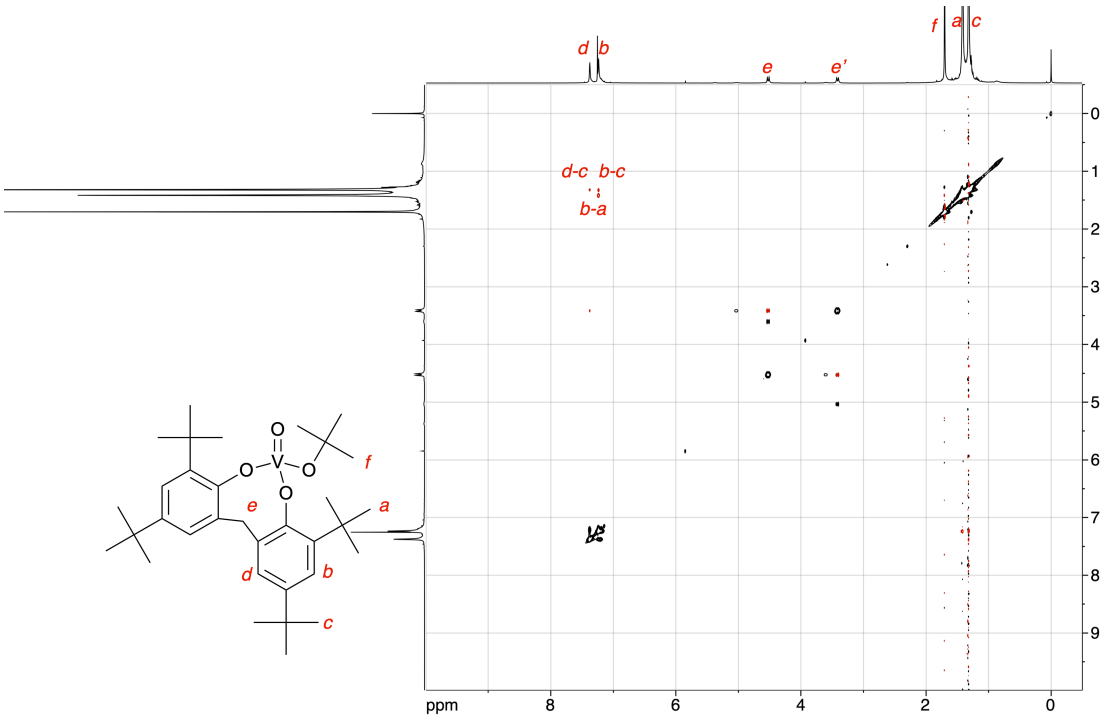

Fig. S23 ^{1}H–^{1}H NOESY NMR spectrum of **3** (500 MHz, $CDCl_3$, 300 K).

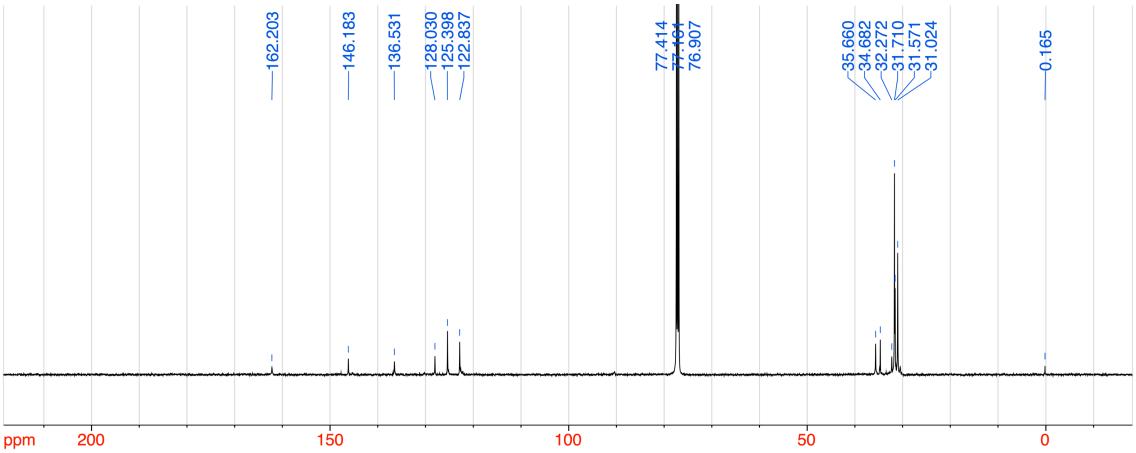

Fig. S24 $^{13}C\{^{1}H\}$ NMR spectrum of **3** ($CDCl_3$, 300 K, 126 MHz).

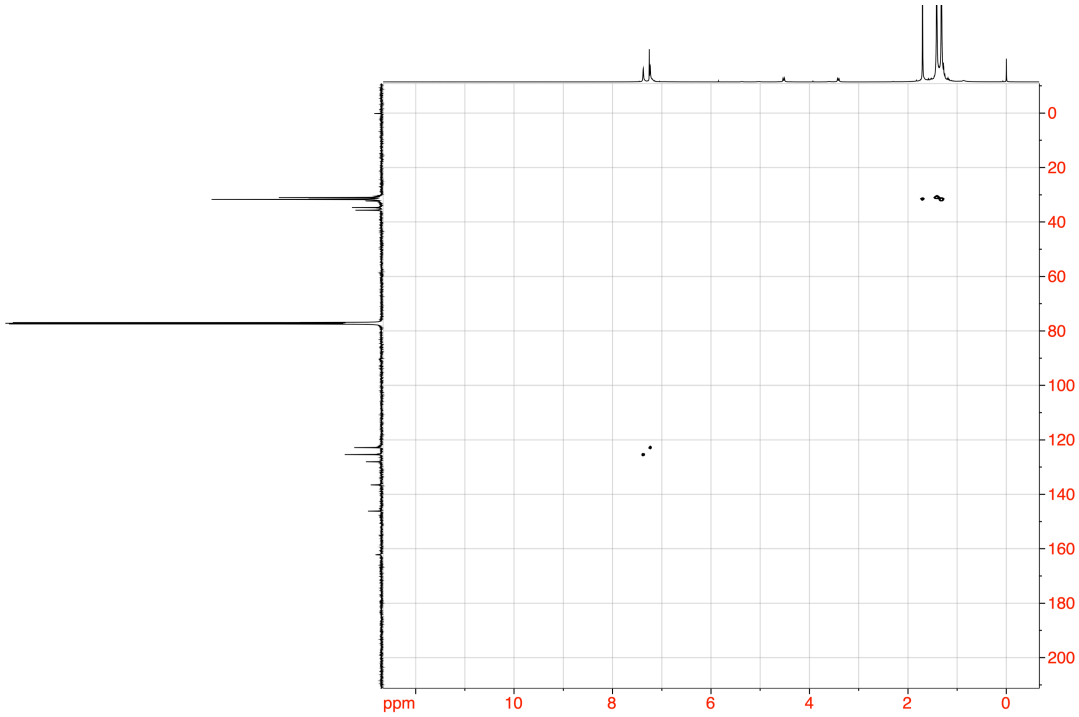

Fig. S25 HSQC NMR spectrum of **3** (^{1}H: 500 MHz, ^{13}C: 126 MHz, $CDCl_3$, 300 K).

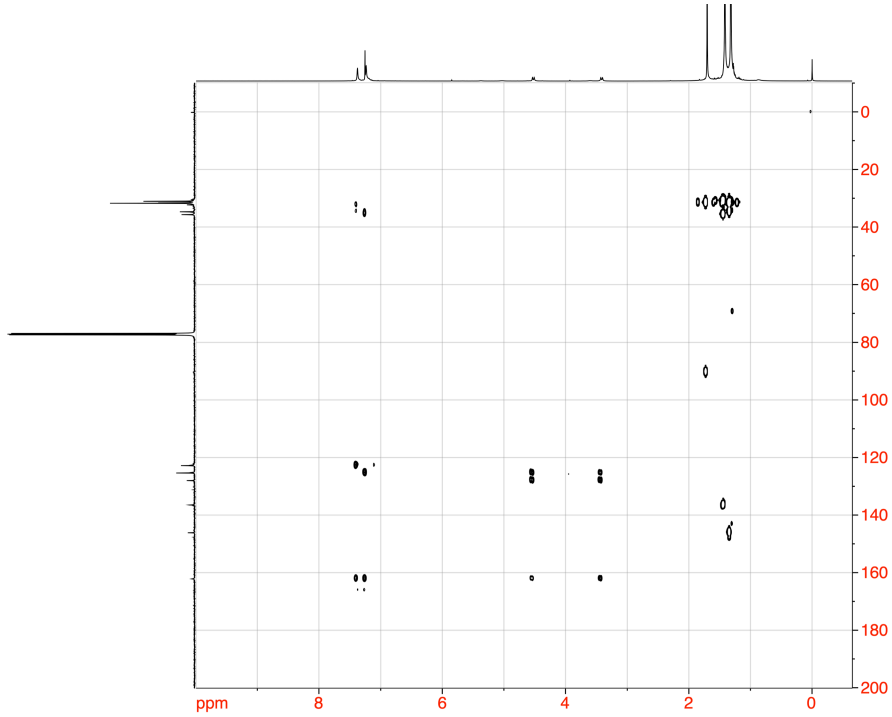

Fig. S26 HMBC NMR spectrum of **3** (^{1}H: 500 MHz, ^{13}C: 126 MHz, $CDCl_3$, 300 K).

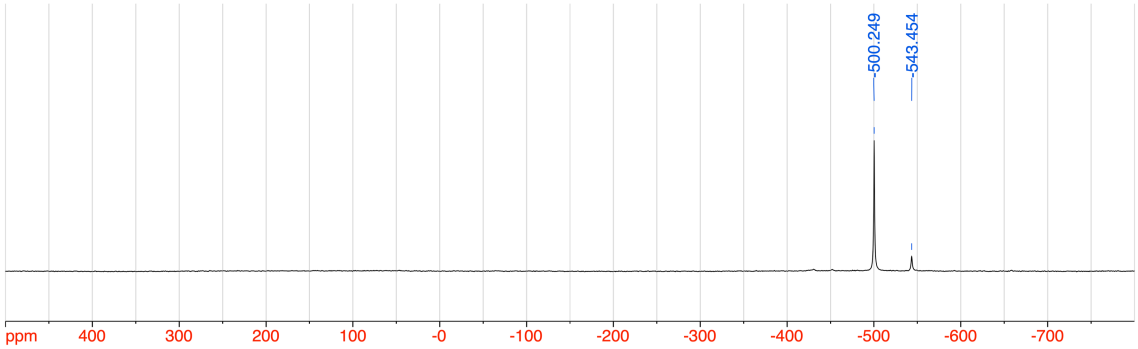

Fig. S27 ^{51}V NMR spectrum of **3** (132 MHz, $CDCl_3$, 300 K).

Comparison of UV-vis spectra of 1 and 3

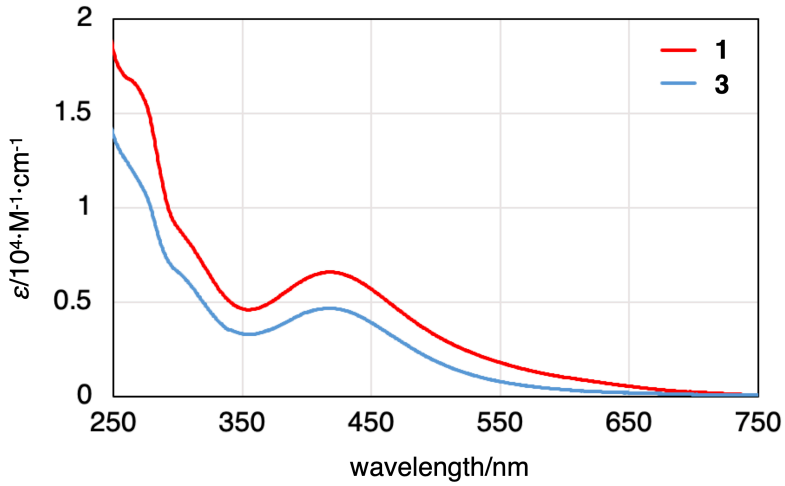

Fig. S28 UV-vis absorption spectra of **1** (red, 1.1×10^{-3} M) and **3** (blue, 3.3×10^{-2} M) in $CHCl_3$ (293 K).

Computational studies

Theoretical calculations for the complexes were performed using Gaussian 16W (revision A.03 and B.01).[S1] The B3LYP density functional theory (DFT) with the B3LYP[S2]/Def2SVP[S3] basis sets were used to optimise the ground-state geometries of the complexes. The geometric parameters of **1** and **2** were optimised from the solid-state structures. The optimisation of the structure of **3** was based on the calculated structures of **1** and **2**. Time-dependent (TD)-DFT calculations were then performed to estimate the energies and oscillator strengths *f* of the 4 lowest-energy singlet and 4 triplet absorptions. In the calculations, the solvent effect of chloroform was evaluated using the Solvent Model based on Density (SMD).[S4] NBO calculations were performed using the NBO 5.0 program package.[S5] The computations of **1** and **2** were performed using the Research Centre for Computational Science, Okazaki, Japan (Project: 20-IMS-C100).

Table S1. Calculated singlet excited state of **1**.

Excited State	Transition	Energy (Wavelength)	Oscillator Strength
S1	HOMO → LUMO (47.8%)	2.5185 eV (492.29 nm)	0.0165
	HOMO-1→ LUMO+1 (1.1%)		
S2	HOMO-1 → LUMO (41.3%)	2.6577 eV (466.51 nm)	0.0001
	HOMO → LUMO+1 (7.9%)		
S3	HOMO-1 → LUMO+1 (46.3%)	2.8493 eV (435.14 nm)	0.0822
	HOMO → LUMO (1.2%)		
	HOMO → LUMO+1 (1.1%)		
S4	HOMO → LUMO+1 (38.5%)	2.8965 eV (428.05 nm)	0.0932
	HOMO-1 → LUMO (7.0%)		
	HOMO-1 → LUMO+1 (1.6%)		
S5	HOMO-2 → LUMO (49.8%)	3.2850 eV (377.43 nm)	0.0010
S6	HOMO-2 → LUMO+1 (49.3%)	3.4086 eV (363.74 nm)	0.0006
S7	HOMO-3 → LUMO (49.4%)	3.4724 eV (357.06 nm)	0.0130
S8	HOMO-3 → LUMO+1 (49.7%)	3.5895 eV (345.40 nm)	0.0018
S9	HOMO → LUMO+2 (49.1%)	3.6306 eV (341.50 nm)	0.0179
S10	HOMO → LUMO+3 (39.0%)	3.7667 eV (329.16 nm)	0.0186
	HOMO-1 → LUMO+2 (9.2%)		

Table S2. Molecular-orbital populations of **1**.

Molecular Orbital	Eigenvalue / eV	MO Population			
		V	O(bridged)	O(terminal)	Aromatic ring (L)
LUMO+3	-1.042	0.50	0.14	0.09	0.20
LUMO+2	-1.342	0.55	0.10	0.14	0.08
LUMO+1	-2.473	0.61	0.14	0.08	0.06
LUMO	-2.661	0.61	0.16	0.02	0.12
HOMO	-5.903	0.05	0.16	0.00	0.67
HOMO-1	-6.167	0.06	0.14	0.01	0.65
HOMO-2	-6.527	0.00	0.00	0.00	0.85
HOMO-3	-6.726	0.00	0.00	0.00	0.82

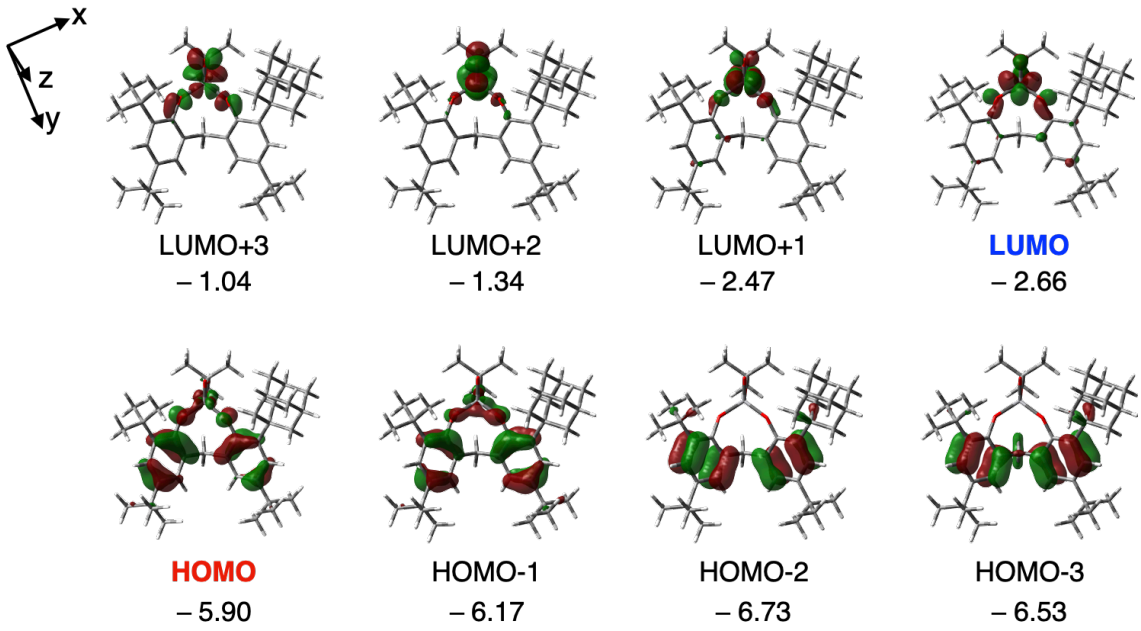

Fig. S29 Frontier molecular orbitals of **1**.

Table S3. Calculated singlet excited state of **2**.

Excited State	Transition	Energy (Wavelength)	Oscillator Strength
S1	HOMO → LUMO (45.4%)	2.1164 eV (585.82 nm)	0.0333
	HOMO-1→ LUMO+1 (3.6%)		
S2	HOMO → LUMO+1 (26.1%)	2.2455 eV (552.14 nm)	0.0045
	HOMO-1 → LUMO (23.1%)		
S3	HOMO-1 → LUMO+1 (45.1%)	2.4824 eV (499.45 nm)	0.1636
	HOMO → LUMO (3.6%)		
S4	HOMO-2 → LUMO (49.1%)	2.8894 eV (429.09 nm)	0.0416
S5	HOMO-2 → LUMO+1 (47.1%)	2.9505 eV (420.22 nm)	0.0203
	HOMO-1 → LUMO (1.3%)		
	HOMO → LUMO+1 (1.2%)		
S6	HOMO-1 → LUMO (21.9%)	3.0196 eV (410.60 nm)	0.2589
	HOMO → LUMO+1 (19.3%)		
	HOMO-3 → LUMO (2.8%)		
	HOMO-2 → LUMO+1 (2.6%)		
S7	HOMO-3 → LUMO (46.8%)	3.0875 eV (401.57 nm)	0.0315
	HOMO → LUMO+1 (1.5%)		
	HOMO-1 → LUMO (1.1%)		

Table S4. Molecular-orbital populations of **2**.

Molecular Orbital	Eigenvalue / eV	MO Population				
		V	O(bridged)	O(terminal)	Cl	Aromatic ring (L)
LUMO+3	-1.287	0.56	0.14	0.12	0.00	0.11
LUMO+2	-1.814	0.62	0.04	0.17	0.11	0.02
LUMO+1	-3.152	0.65	0.11	0.03	0.07	0.12
LUMO	-3.211	0.64	0.13	0.02	0.05	0.13
HOMO	-6.313	0.08	0.11	0.01	0.05	0.64
HOMO-1	-6.514	0.10	0.08	0.00	0.02	0.66
HOMO-2	-6.820	0.00	0.00	0.00	0.00	0.84
HOMO-3	-7.022	0.00	0.00	0.00	0.00	0.80

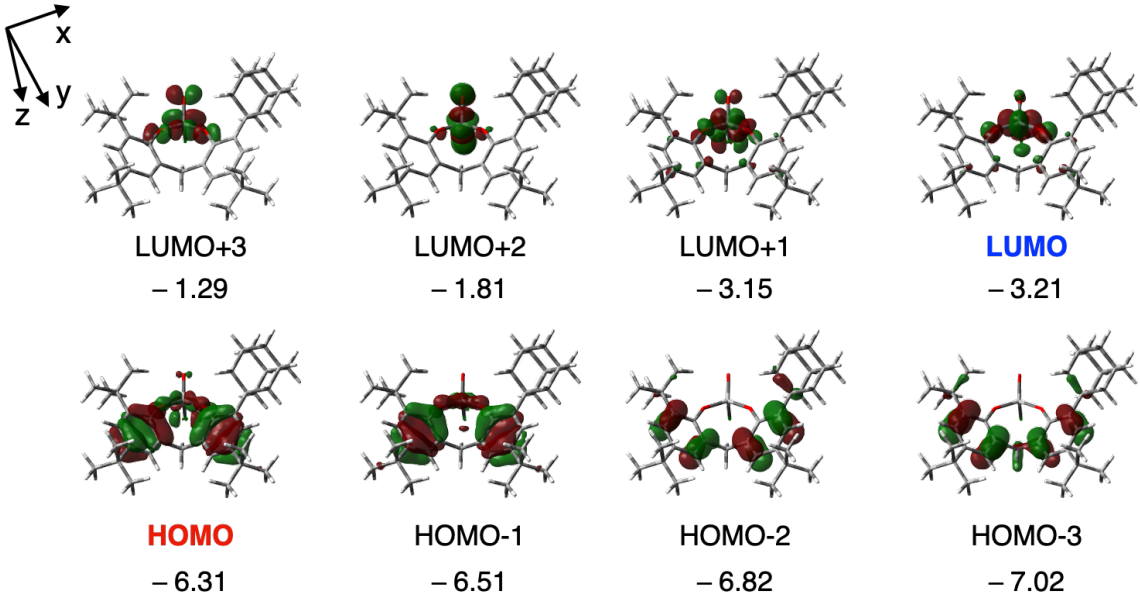

Fig. S30 Frontier molecular orbitals of **2**.

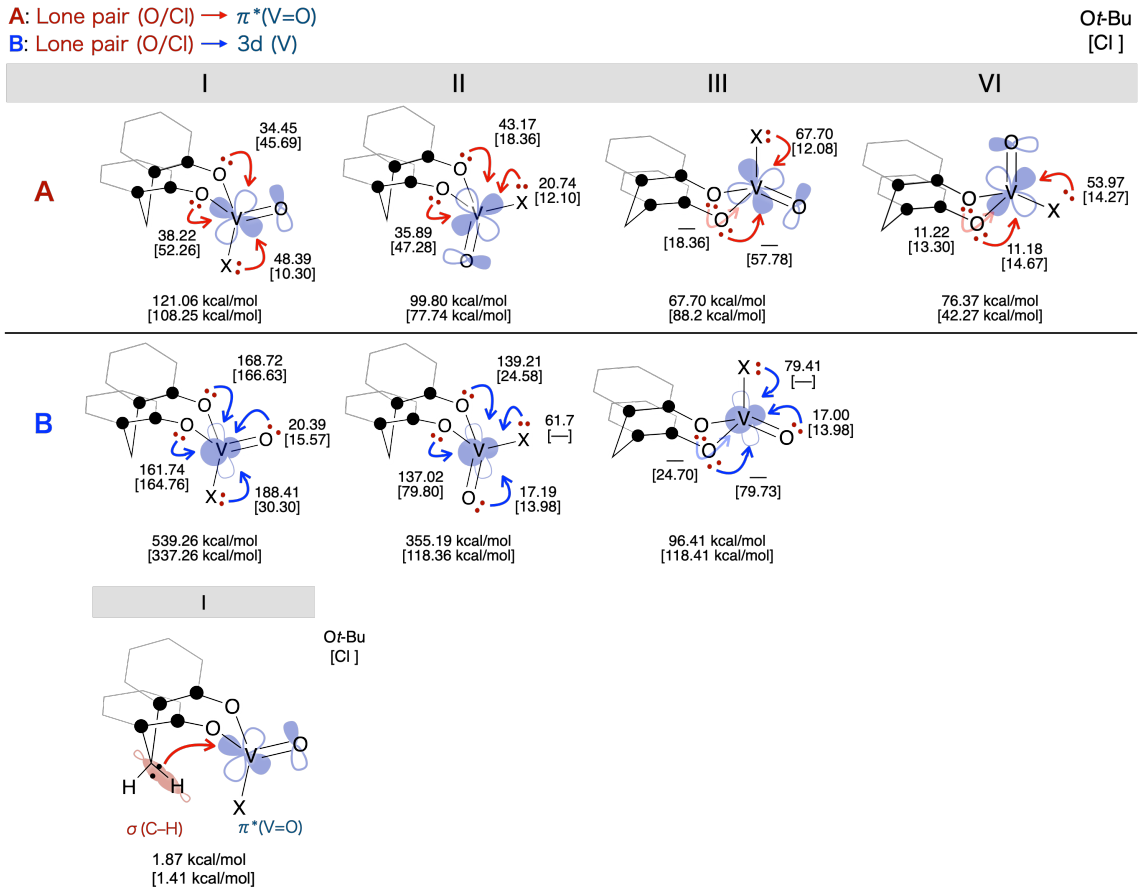

Fig. S31 Second-order perturbation of **I**-**VI**.

Table S5. Second-order perturbation of **I**-**VI**.

		I	II	III	VI
A	X = O*t*-Bu	121.06	99.80	67.70	76.37
	X = Cl	108.25	77.74	88.20	42.27
B	X = O*t*-Bu	539.26	355.19	96.41	
	X = Cl	337.26	118.36	118.41	
A + B	X = O*t*-Bu	660.32	454.90	164.11	76.37
	X = Cl	445.51	196.10	206.61	42.27

[a] Calculated at the B3LYP/Def2SVP level of theory. [b] In kcal mol^{-1}

Table S6. Molecular-orbital populations of **3**.

Molecular Orbital	Eigenvalue / eV	MO Population			
		V	O(bridged)	O(terminal)	Aromatic ring (L)
LUMO+3	-0.495	0.55	0.15	0.11	0.10
LUMO+2	-1.021	0.56	0.11	0.15	0.04
LUMO+1	-1.328	0.61	0.16	0.05	0.08
LUMO	-2.464	0.64	0.14	0.03	0.13
HOMO	-5.911	0.04	0.20	0.00	0.64
HOMO-1	-6.164	0.08	0.13	0.00	0.66
HOMO-2	-6.542	0.00	0.00	0.00	0.89
HOMO-3	-6.768	0.00	0.01	0.00	0.85

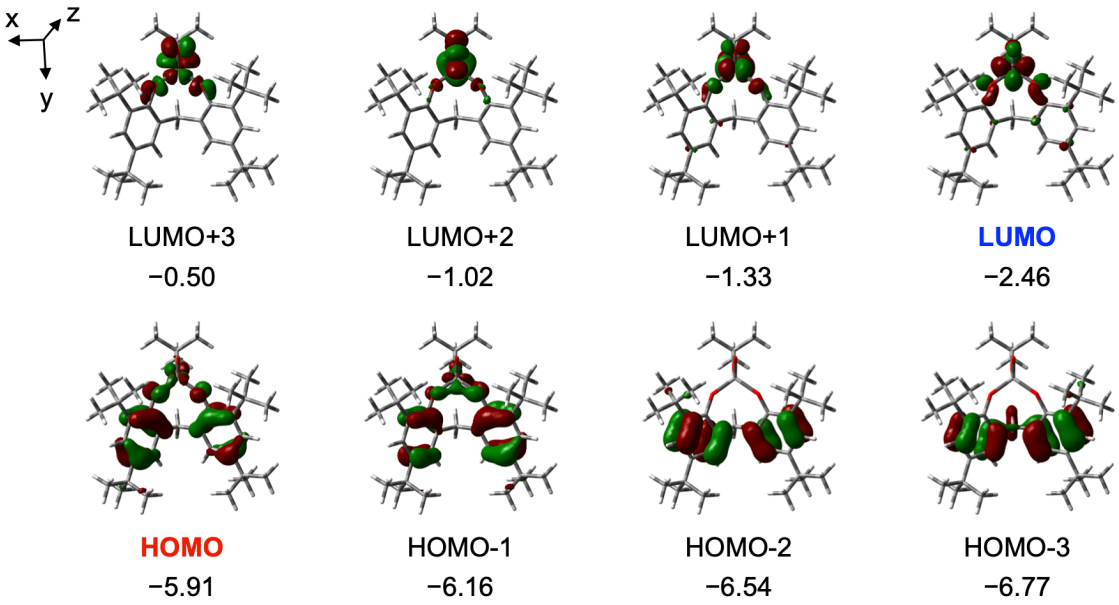

Fig. S32 Frontier molecular orbitals of **3**.

ATR-IR spectra of 1 and 2

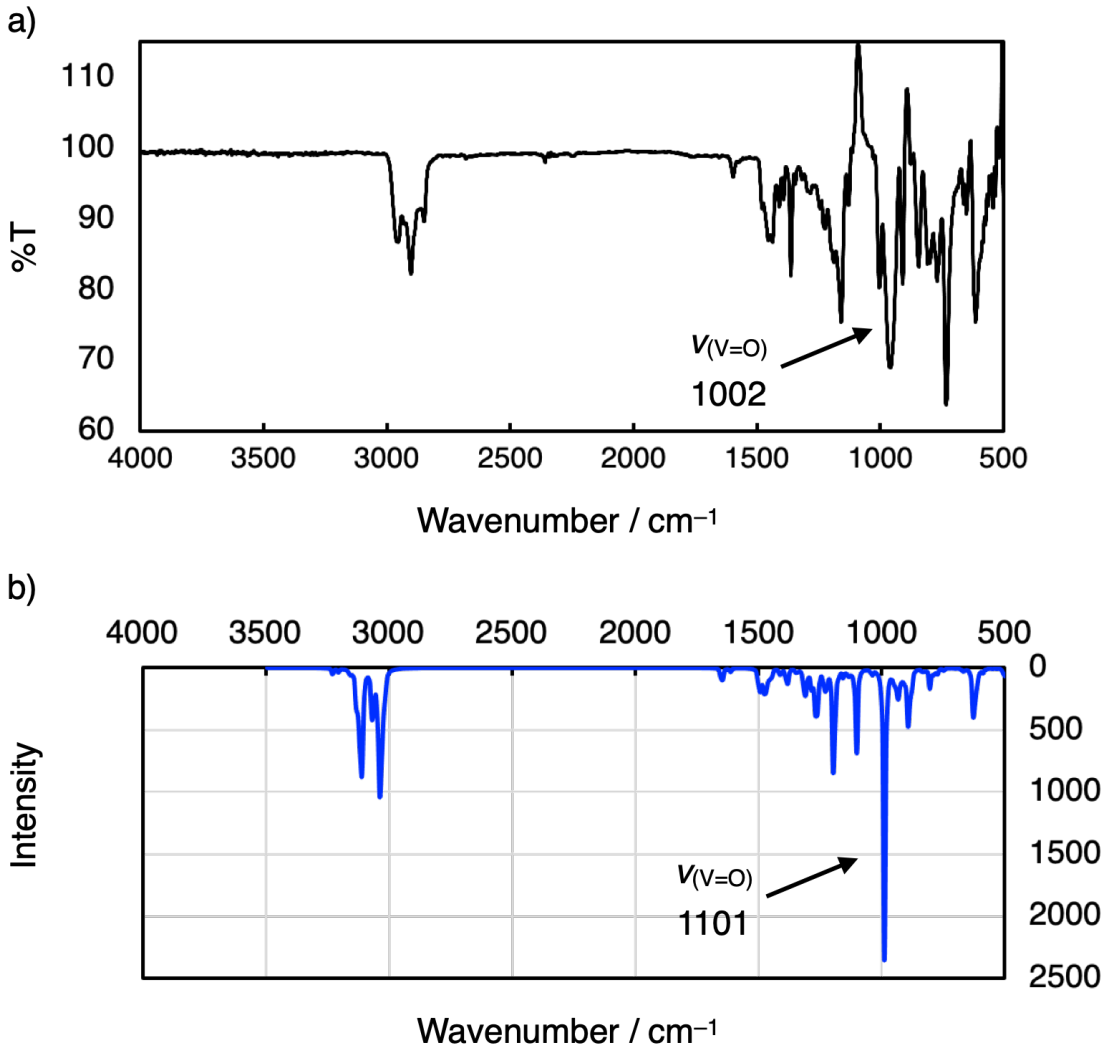

Fig. S33 a) Solid-state ATR-IR spectrum of [V(O)(O*t*-Bu)**L**]. b) IR spectrum calculated for the [V(O)(O*t*-Bu)**L**] (drawn by using the GaussView 5.0 software, half-width at half-maximum = 4 cm^{-1}, without scaling) (B3LYP/Def2SVP).

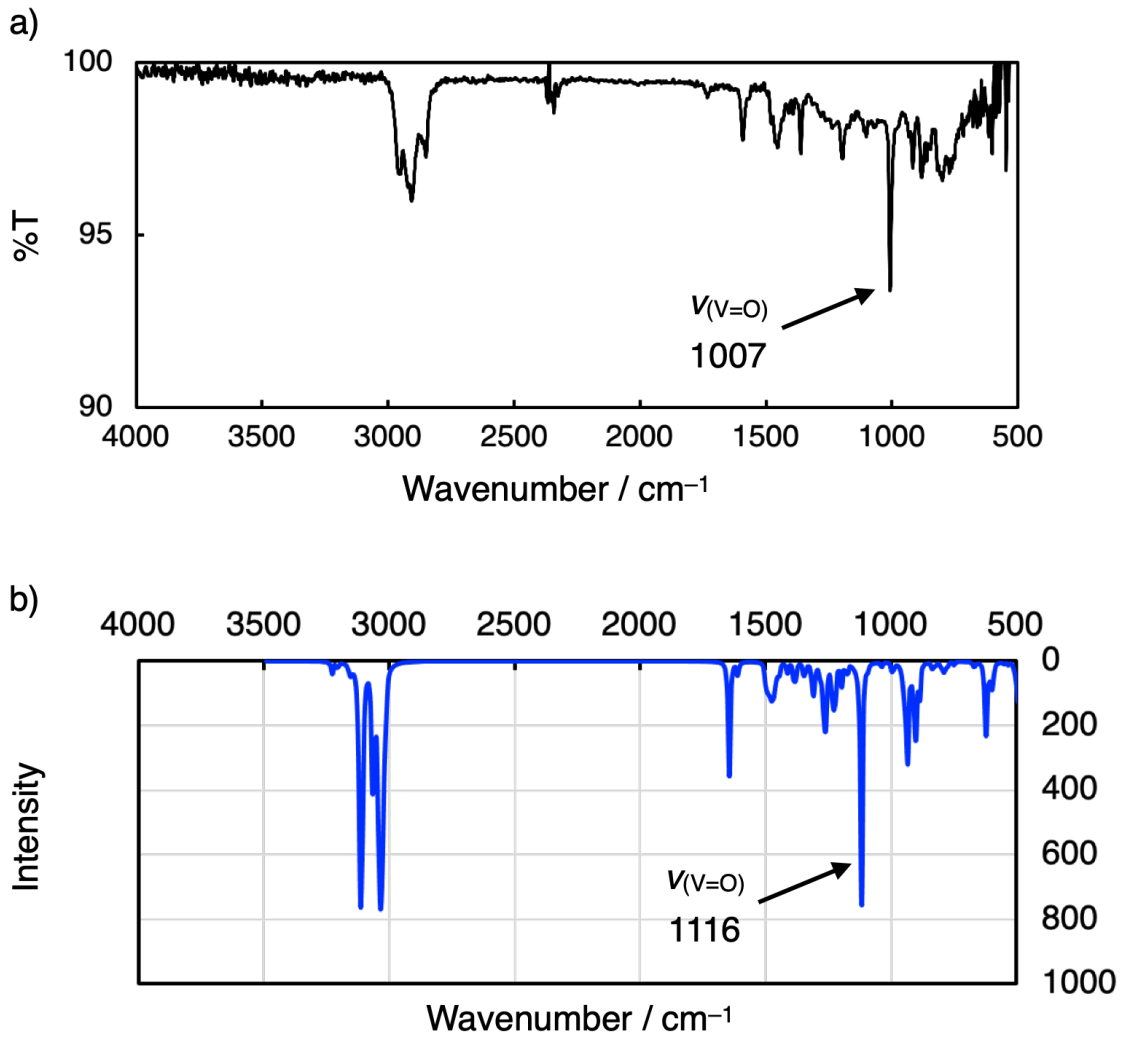

Fig. S34 a) Solid-state ATR-IR spectrum of [V(O)Cl**L**]. b) IR spectrum calculated for the [V(O)Cl**L**] (drawn by using the GaussView 5.0 software, half-width at half-maximum = 4 cm^{-1}, without scaling) (B3LYP/Def2SVP).

X-Ray crystallographic analysis of *rac*-[V(O)(O*t*-Bu)L] (1) and *rac*-[V(O)ClL] (2)

Single crystals of **1** and **2** were grown by slow evaporation of their solutions ($CHCl_3$/*n*-hexane for **1** and benzene for **2**) at room temperature in a nitrogen-filled glovebox. Intensity data were collected on a Rigaku XtaLAB PRO MM007DW PILATUS diffractometer using Cu Kα radiation, and the obtained data were calculated with Olex2[S6] 1.2.10 (OlexSys Ltd., 2018) software. The structures were solved with the ShelXT[S7] structure solution program using Intrinsic Phasing or the ShelXL[S8] refinement package using Least Squares minimization. All hydrogens atoms were geometrically arranged and refined using a riding model.

CCDC-2210598 (**1**) and CCDC-2210585 (**2**) contain supplementary crystallographic data for this paper. These data are available free of charge from The Cambridge Crystallographic Data Centre via www.ccdc.cam.ac.uk/data_request/cif.

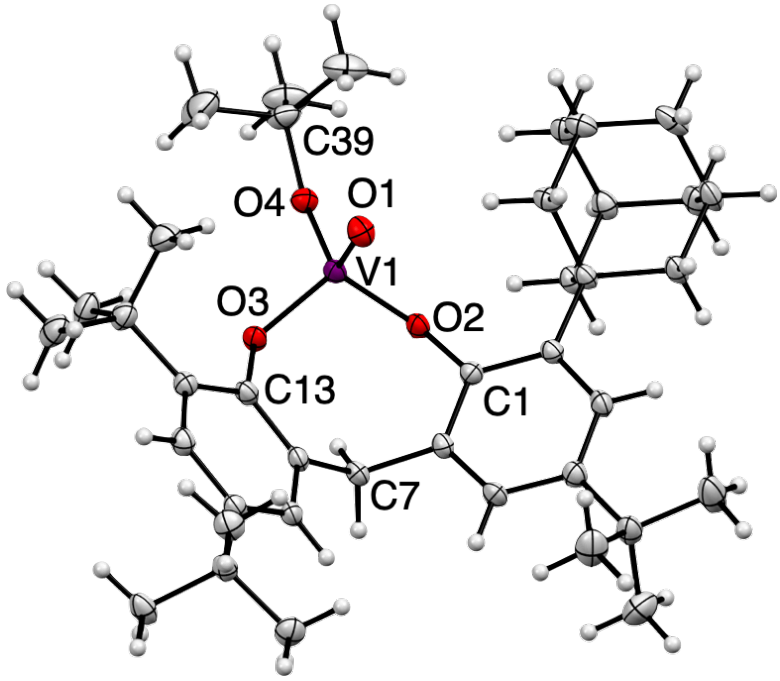

Fig. S35 Molecular structure of *rac*-[V(O)(O*t*-Bu)**L**] (**1**). Thermal displacement ellipsoids are set at the 50% probability level. Selected bond lengths [Å] and angles [°]; V(1)=O(1) 1.5865(10), V(1)–O(2) 1.7902(10), V(1)–O(3) 1.7892(10), V(1)–O(4) 1.7397(10); O(1)–V(1)–O(2) 108.97(5), O(1)–V(1)–O(3) 107.12(5), O(1)–V(1)–O(4) 111.80(5), O(2)–V(1)–O(3) 109.69(4), O(3)–V(1)–O(4) 110.16(5), O(4)–V(1)–O(2) 109.07(5), V(1)–O(2)–C(1) 127.67(5), V(1)–O(3)–C(13) 129.91(5).

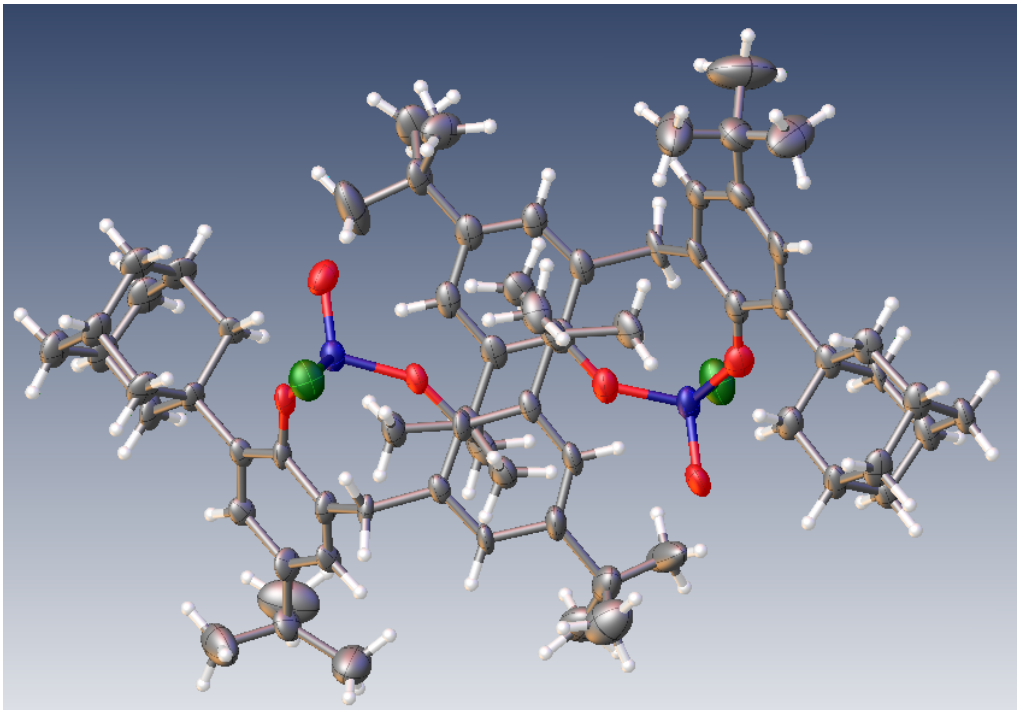

Fig. S36 Molecular structure of *rac*-[V(O)Cl**L**] (**2**). Thermal displacement ellipsoids are set at the 50% probability level. Two crystallographically independent molecules of **2** were found in the unit cell. Selected bond lengths [Å] and angles [°]; Molecule A: V(1)=O(1) 1.581(10), V(1)–O(2) 1.771(10), V(1)–O(3) 1.744(9), V(1)–Cl(2) 2.167(11); O(1)–V(1)–O(2) 107.9(5), O(1)–V(1)–O(3) 107.0(4), O(1)–V(1)–Cl(2) 107.6(5), O(2)–V(1)–O(3) 109.7(5), O(3)–V(1)–Cl(2) 112.5(5), Cl(2)–V(1)–O(2) 111.8(4), V(1)–O(2)–C(1) 138.9(9), V(1)–O(3)–C(21) 144.8(8); Molecule B: V(2)=O(4) 1.600(11), V(2)–O(5) 1.753(16), V(2)–O(6) 1.764(11), V(2)–Cl(1) 2.202(10); O(4)–V(2)–O(5) 109.6(5), O(4)–V(2)–O(6) 110.8(5), O(4)–V(2)–Cl(1) 109.0(5), O(5)–V(2)–O(6) 107.5(8), O(6)–V(2)–Cl(1) 107.6(5), Cl(1)–V(2)–O(5) 112.2(4), V(2)–O(5)–C(36) 146.1(11), V(2)–O(6)–C(56) 149.9(8).

Table S7. Crystal Data for **1** and **2**.

	***rac*-[V(O)(O*t*-Bu)L] (1)**	***rac*-[V(O)ClL] (2)**
Formula	$C_{39}H_{57}O_4V$	$C_{35}H_{48}ClO_3V$
Formula weight	640.78	603.12
Crystal dimensions/mm^3	0.05 × 0.05 × 0.1	0.11 × 0.14 × 0.18
Temperature/K	93.15	93.15
Crystal system	triclinic	Orthorhombic
Space group	*P*-1 (#2)	$Pmc2_1$ (#26)
Lattice parameters		
a/Å	11.3936(3)	10.4288(2)
b/Å	13.2903(3)	27.1835(4)
c/Å	13.4060(3)	11.2290(2)
α/deg	75.111(2)	90
β/deg	69.895(2)	90
γ/deg	75.358(2)	90
V/Å^3	1811.79(8)	3183.32(10)
Z	2	4
D_{calcd}/g·cm^{-3}	1.175	1.258
μ/mm^{-1}	2.568	3.623
θ/deg	6.998 to 146.834	6.504 to 144.2
No. of reflections	17500	35727
Independent reflections	7043	5925
R_{int}	0.0241	0.0384
Completeness to θ/%	99.4	100
R_1 [$I > 2\sigma(I)$]	0.0337	0.0712
wR_2 (all data)	0.0922	0.2112
Largest diff. peak/e·Å^{-3}	0.26	0.55
Largest diff. hole/e·Å^{-3}	–0.39	–0.70
Goodness-of-fit on F^2	1.082	1.065

References

(S1) M. J. Frisch, G. W. Trucks, H. B. Schlegel, G. E. Scuseria, M. A. Robb, J. R. Cheeseman, G. Scalmani, V. Barone, G. A. Petersson, H. Nakatsuji, X. Li, M. Caricato, A. V. Marenich, J. Bloino, B. G. Janesko, R. Gomperts, B. Mennucci, H. P. Hratchian, J. V. Ortiz, A. F. Izmaylov, J. L. Sonnenberg, D. Williams-Young, F. Ding, F. Lipparini, F. Egidi, J. Goings, B. Peng, A. Petrone, T. Henderson, D. Ranasinghe, V. G. Zakrzewski, J. Gao, N. Rega, G. Zheng, W. Liang, M. Hada, M. Ehara, K. Toyota, R. Fukuda, J. Hasegawa, M. Ishida, T. Nakajima, Y. Honda, O. Kitao, H. Nakai, T. Vreven, K. Throssell, J. A. Montgomery, Jr., J. E. Peralta, F. Ogliaro, M. J. Bearpark, J. J. Heyd, E. N. Brothers, K. N. Kudin, V. N. Staroverov, T. A. Keith, R. Kobayashi, J. Normand, K. Raghavachari, A. P. Rendell, J. C. Burant, S. S. Iyengar, J. Tomasi, M. Cossi, J. M. Millam, M. Klene, C. Adamo, R. Cammi, J. W. Ochterski, R. L. Martin, K. Morokuma, O. Farkas, J. B. Foresman and D. J. Fox, Gaussian, Inc., Wallingford CT, 2016.

(S2) S. Grimme, *J. Chem. Phys.*, 2006, **124**, 034108.

(S3) F. Weigend and R. Ahlrichs, *Phys*. *Chem*. *Chem*. *Phys*., 2005, **7**, 3297-3305.

(S4) A. V. Marenich, C. J. Cramer and D. G. Truhlar, *J*. *Phys*. *Chem*. *B*, 2009, **113**, 6378-6396.

(S5) E. D. Glendening, J. K. Badenhoop, A, E. Reed, J. E. Carpenter, J. A. Bohmann, C. M. Morales and F. Weinhold, NBO 5.0, Theoretical Chemistry Institute, University of Wisconsin, Madison, WI, 2001.

(S6) O. V. Dolomanov, L. J. Bourhis, R. J. Gildea, J. A. K. Howard and H. Puschmann, *J*. *Appl*. *Cryst*. 2009, **42**, 339.

(S7) G. M. Sheldrick, *Acta Cryst*. 2015, **A71**, 3.

(S8) G. M. Sheldrick, *Acta Cryst*. 2015, **C71**, 3.